DESIGN, SIMULATION, AND CONSTRUCTION OF A VERSATILE ELECTROCHEMICAL CELL FOR IN-OPERANDO X-RAY DIFFRACTION STUDIES

Lioren Bessone Jofre[1], Andrea Calderon[1], Esteban Franceschini[2] y Sergio Ceppi[1]

[1]IFEG, Facultad de Matemática, Astronomía, Física y Computación, Universidad Nacional de Córdoba, Argentina

[2] INFIQC, Departamento de Fisicoquímica, Facultad de Ciencias Químicas, Universidad Nacional de Córdoba, Argentina

Introduction

In an electrochemical cell, very complex processes occur in which molecules and solids exchange electrons, requiring detailed measurement of the dynamics of the reactions as they are triggered. The way to do this is to collect as much information as possible while the electrochemical reaction is occurring. To address these needs, efforts have been directed toward reliable, fast and easy-to-perform in-operating measurements. Advances in cell design, such as emerging plastic cells, have increased the implementation of in-operando XRD characterization of new electrode materials for energy storage.

In this work, the design and construction of a cell for in-operating electrochemical X-ray diffraction experiments was carried out. The design was made by modeling and 3D printing, and then machined in AISI 316L steel. This prototype has two parallel electrodes and a septum that allows the injection of gases, reagents and even a third electrode (reference) with ease and maintaining the tightness of the system, which makes it very versatile for a wide range of applications. This cell was tested with several ex situ, in situ and in-operating experiments analyzing the formation of surface oxides during the application of an electrochemical potential pulse. It was found that this cell maintains tightness for at least 3 days and allows performing a variety of electrochemical experiments (cyclic voltammetry and chronoamperometry) while obtaining X-ray diffractograms with excellent resolution.

Exploded view of the cell in operation

The working electrode is placed inside an electrically conductive cup that also contains a series of springs and separators that will be mentioned later. A celgard separator is placed over the working electrode to allow ionic conductivity avoiding short-circuit with the counter electrode.

For good electrical contact, the counter electrode of the cell has to be pressed tightly against the metalized window through which radiation enters, not the cell cup button, as it short-circuits. To ensure both, we decided to slightly lift the circular center step in Part 3 (Figure 4a) and introduce an insulating ring into the design to prevent shorting while helping to align the cell components during assembly. This part is slightly offset from the symmetry axis to allow good alignment between the test cell, the window, and the radiation beam footprint.

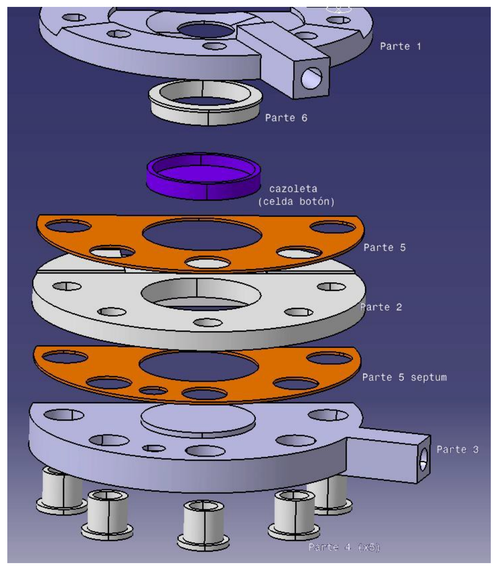

Internal cell design

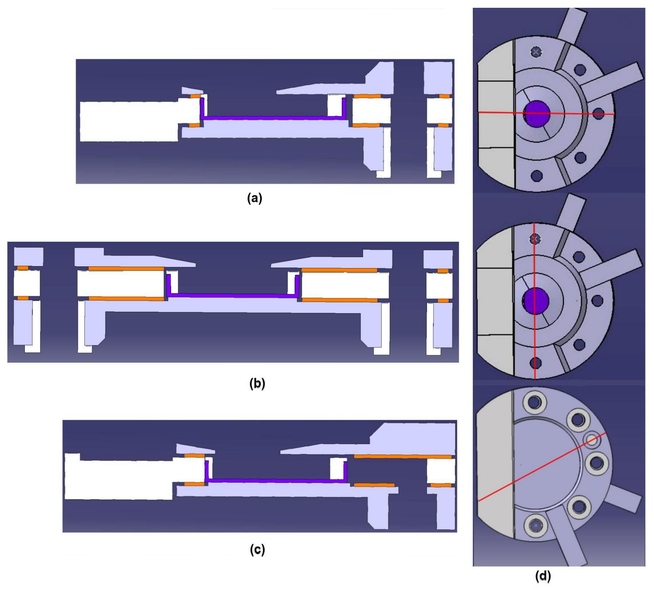

In Figure 6b you can see how the bushing system that isolates the screws works. In Figure 6c the injection system can be seen in detail, assembling the cell with Part 2 septum. In the visible hole of Part 3, the thread of the septum is housed, matching the electrical potential of the septum with this electrode, leaving an opening for gases or liquids injected from the outside to flow into the electrochemical system. This system can be blocked by assembling the cell with Part 2, eliminating the injection channel. In addition, in a) as well as in b) and c) it can be seen that the location of the rubber (orange) is evidence that the system is hermetic.

Simulations Results

We simulate a stack to study the beam just after it passes through the graphite.

through the graphite. The graph in Figure 5.6 shows the transmittance as a function of penetration depth for the elements: kapton, nickel, lithium, celgard and graphite stacked in the in-situ cell for an incidence angle of 90°. From the graph we can see that for a total thickness of the components of 0.10358cm and an angle of incidence of 90° the resulting transmittance is 0.792.

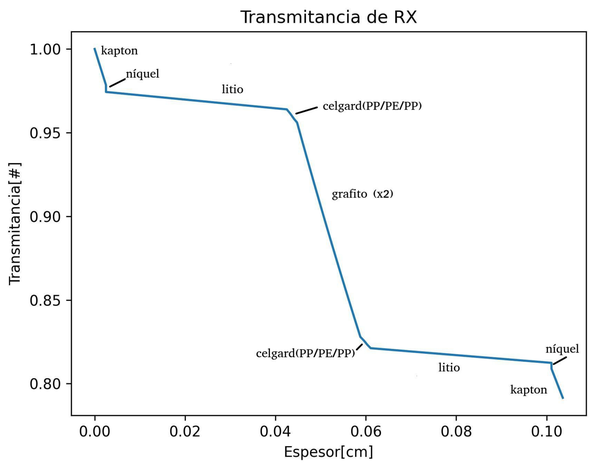

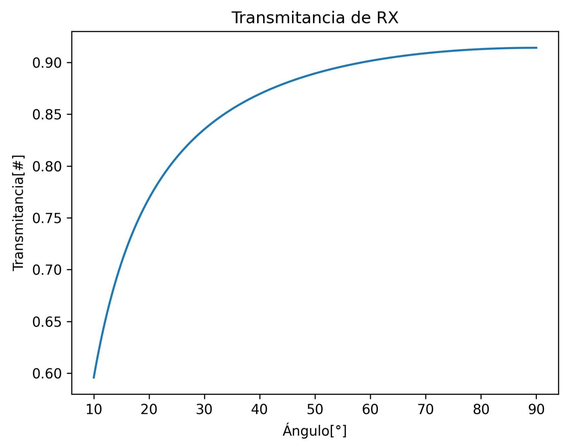

Considering the same stack of elements but analyzing the transmittance as a function of the angle instead of the thickness, we obtain a graph like the one in Figure 5.7. In which we can see that for an angle of =21.7° the transmittance takes a value of 0.532. While for =90° we recover the transmittance value of 0.792, coinciding with the thickness graph for the maximum thickness as expected.

Electrochemical Experiments

In a constant current charge, the anode stores lithium ions, as long as it can do so, at the assigned rate. The rate at which it can do so. The newly assembled cell has a potential of 1.5V (initial work function difference between lithium and graphite), in the first half cycle, with a current of -50 µA, a potential drop occurs between electrodes and the cell discharges to 0.05V. In the second half cycle, with an applied current of +50 µA, the cell is charged again reaching a potential of 1.5V (cutoff set in the cycler). If we compare we can associate the first semicycle with the charging of the graphite anode (decreasing the potential difference between electrodes) and the second semicycle with the reverse process of discharging the graphite anode (respective increase of the potential difference). The charging and discharging processes are associated with the intercalation and deintercalation of lithium respectively, showing that the cell is working properly.

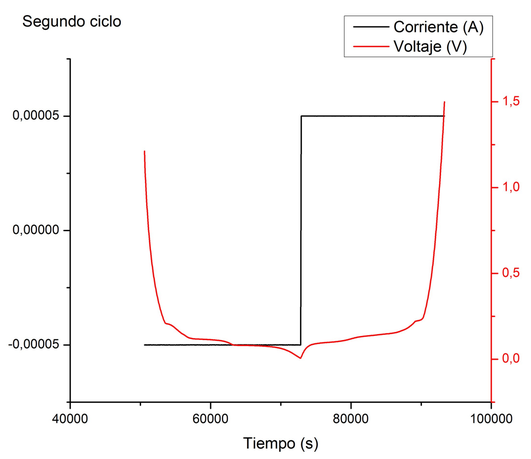

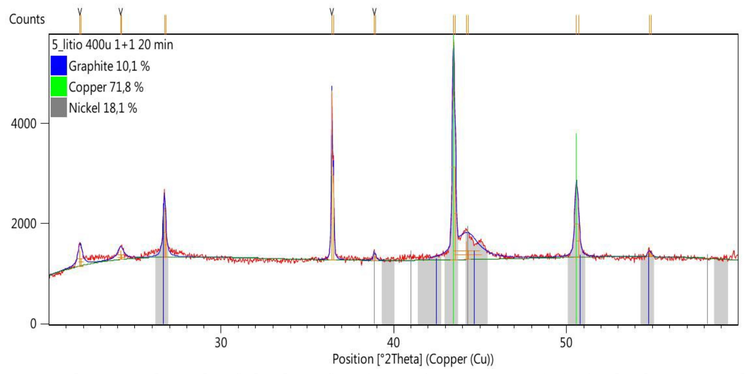

The cell test yielded the diffractogram in Figure 5.24 where a sweep in 2 is observed between 20° and 60°. At 2B =(26.696 ± 0.002)° one can clearly see the graphite peak that we expected to find, evidencing that the aperture cone that houses the window in Part 1 combined with a non-negligible effective area effective area raises signal from B =10° (see Figure 2.17).

Using the wavelength of the line for Cu-K (see section 2.6.1), the bragg angle obtained from the diffractogram of the Cu-K obtained from the diffractogram of Figure 5.24, the diffraction order for that peak, and equation 2.14.1. and equation 2.14 we obtain an interplanar distance of d 3.35 Å in coincidence with the coinciding with what was explained in 3.3. The aforementioned medium intensity peak is followed by another low intensity peak at is followed by another low intensity peak at (54.79± 0.002)°.

Conclusions

One of the main differences between the cell designed in this work with the state of the art is its adaptability to PANalytical equipment thanks to its truncated disk shape and lightweight design. The latter is made possible by the use of a Kapton™ window, a button cell cup with spacers instead of a spring, and the use of a commercial septum that can act as a third electrode and at the same time as a liquid and gas injection control system.

This cell takes advantage of the equipment's factory alignment system, which is why it's mounting on the diffractometer is fast (compared to, for example, a clamping foot, which depends on the surface where it is supported). Fine alignment requires determining the number of spacers to be used to match the alignment plane of the equipment with that of the sample depending on the thickness of the materials contained inside.